



Multipass-assisted dual-comb gas sensor for multi-species detection using a free-running fiber laser

Ke Xu^{1,2} · Xin Zhao³ · Zhen Wang^{1,2} · Jie Chen³ · Ting Li³ · Zheng Zheng³ · Wei Ren^{1,2} 

Received: 20 July 2019 / Accepted: 20 December 2019 / Published online: 11 February 2020
© Springer-Verlag GmbH Germany, part of Springer Nature 2020

Abstract

We demonstrated a multipass-assisted dual-comb gas sensor for the simultaneous and sensitive detection of C₂H₂ and NH₃ near 1.5 μm using a single free-running fiber laser. Two pulse trains generated from the shared cavity in the passively mode-locked fiber laser ensure the mutual coherence and common-mode noise rejection. One of the comb pulse trains passed through an open-path multipass cell with an effective path length of 4 m. A synchronized acquisition technique was adopted for more efficient interferogram acquisition compared with the conventional continuous acquisition method. At an acquisition time of 1.5 s, we obtained a signal-to-noise ratio of more than 600 by 1500 averages of the acquired spectrum of 0.1% C₂H₂. Pressure broadening of C₂H₂ and NH₃ in the frequency range of 6503–6530 cm⁻¹ between 0.1 and 1 bar were captured by the dual-comb sensor. Finally, the free-running fiber laser-based dual-comb sensor successfully analyzed the C₂H₂/NH₃ mixtures, enabling real-time gas sensing without using complex optical and electronic feedback systems.

1 Introduction

Optical frequency comb (OFC) with equally spaced and mutually coherent spectral lines over a broadband spectrum is becoming a significant research focus in laser spectroscopy [1–4]. Among different OFC-based spectroscopic techniques [5–7], dual-comb spectroscopy (DCS) has been recently proposed for high-resolution molecular spectroscopy using two OFCs with a slight difference in their repetition frequencies [8]. Such a method has the potential of replacing conventional Fourier-transform spectroscopy with advantages of ultrahigh resolution and ultrafast speed.

DCS is normally performed using a pair of OFCs generated by two ultrafast mode-locked lasers with the stabilized pulse repetition frequency (f_r) and carrier-envelope offset

frequency (f_{ceo}). The repetition frequencies of the two comb trains are synchronized with a small frequency difference Δf . In the frequency domain, such a Δf causes multi-heterodyne of adjacent comb teeth from both pulse trains, thus down-converting the optical spectrum to the radio frequency (RF) region. In the time domain, the interferogram containing the spectral signature is acquired and Fourier-transformed to retrieve the molecular spectra.

However, the use of two independent mode-locked laser cavities requires sophisticated and expensive phase-locking systems to ensure the mutual coherence with respect to Δf between the comb pair. Additionally, precise electronic feedbacks and stable environments are commonly needed to maintain the f_r and f_{ceo} of those two mode-locked lasers [8, 9]. Hence, several approaches such as the use of two self-referenced OFCs locked to a common diode laser [10], post-processing of data correction [11, 12] and adaptive sampling [13] were proposed to improve the detection performance. Although the relative instability could be corrected substantially, the complexity and cost still remain high for dual-laser comb sources. Additionally, electro-optic-modulator (EOM) based comb system may achieve a good mutual coherence [14], which however is prone to the limited spectral coverage and resolution, since the optical sampling by cavity tuning (OSCAT) scheme is adopted with an unbalanced non-static interferometer configuration.

✉ Zheng Zheng
zhengzheng@buaa.edu.cn

✉ Wei Ren
renwei@mae.cuhk.edu.hk

¹ Department of Mechanical and Automation Engineering, The Chinese University of Hong Kong, New Territories, Hong Kong SAR, China

² Shenzhen Research Institute, The Chinese University of Hong Kong, New Territories, Hong Kong SAR, China

³ School of Electronic and Information Engineering, Beihang University, Beijing 100083, China

An alternative way of achieving less-complicated and low-cost DCS is to make use of intracavity passive mutual coherence [4]. Two trains of asynchronous OFC pulses with an offset f_r could be generated by one single laser cavity [15–20]. Particularly, phase-coherent free-running dual combs could be generated from a dual-wavelength mode-locked laser [15, 21]. The frequency difference Δf between the generated two pulse trains is determined by the intracavity group velocity dispersion. A free-running DCS system with a picometer resolution has been demonstrated using an erbium-doped fiber (EDF) laser [22]. In addition, the DCS experiment using a single thulium-doped dual-wavelength mode-locked laser was also demonstrated near 2 μm [23].

Although the previous studies demonstrated the potential of using single-laser-cavity-based DCS for molecular spectroscopy, methods of performing sensitive and multi-species gas detection using this laser scheme have not been fully researched. In this paper, we demonstrate a dual-comb gas sensor for the sensitive and simultaneous detection of C_2H_2 and NH_3 using one single erbium-doped free-running fiber laser combined with a multipass open-path configuration. DCS used in this scheme is designed to cover the near-infrared range of 1530–1550 nm for C_2H_2 and NH_3 detection. To improve the detection sensitivity, we merge DCS with the multipass technology to significantly extend the absorption path length of the gas sensor. We also investigate the sensor performance at different gas pressures. Additionally, a synchronized acquisition technique is applied with the sampling frequency determined by the repetition frequency of one comb, enabling the real-time multi-species detection.

2 Sensor configuration

Figure 1 depicts the schematic of the proposed dual-comb multipass gas sensor with a free-running fiber laser. The erbium-doped fiber ring laser was mode-locked using a single-wall carbon nanotube saturable absorber (SWNT-SA) [24]. The laser was pumped by a 980-nm continuous-wave laser (II–VI LC96Z400) and then formed a unidirectional oscillation of the pulses inside the cavity by a hybrid 980/1550 nm wavelength division multiplexer/isolator (WDM/ISO). When the laser is pumped above the mode-locking threshold, the dual-wavelength oscillation of the laser is generated by the effects of intracavity birefringence and polarization-dependent loss controlled by a polarization controller (PC). The laser cavity consisted of a 0.4-m erbium-doped fiber (EDF Er110) as the amplifying fiber [25] and a 3.2-m single-mode fiber. An in-line polarization beam splitter (PBS) with a 0.25-m polarization maintaining fiber was also placed in the cavity to ensure the polarization state of dual-comb pulse trains' output. Further information of the laser source could be found elsewhere [22].

Figure 2a presents the typical laser output with two spectral peaks centered at 1533 nm and 1543 nm, respectively. The typical 3-dB spectral bandwidth is determined to be both around 2 nm. As monitored by the photodetector (Thorlabs PDA05CF2) and the spectrum analyzer (Rohde-Schwarz FPC-1000), the repetition frequencies were measured to be 61.15 MHz with a frequency difference of 1 kHz. The two repetition frequencies normally vary by ~ 10 Hz in 10 min but always drift in the same direction by the same

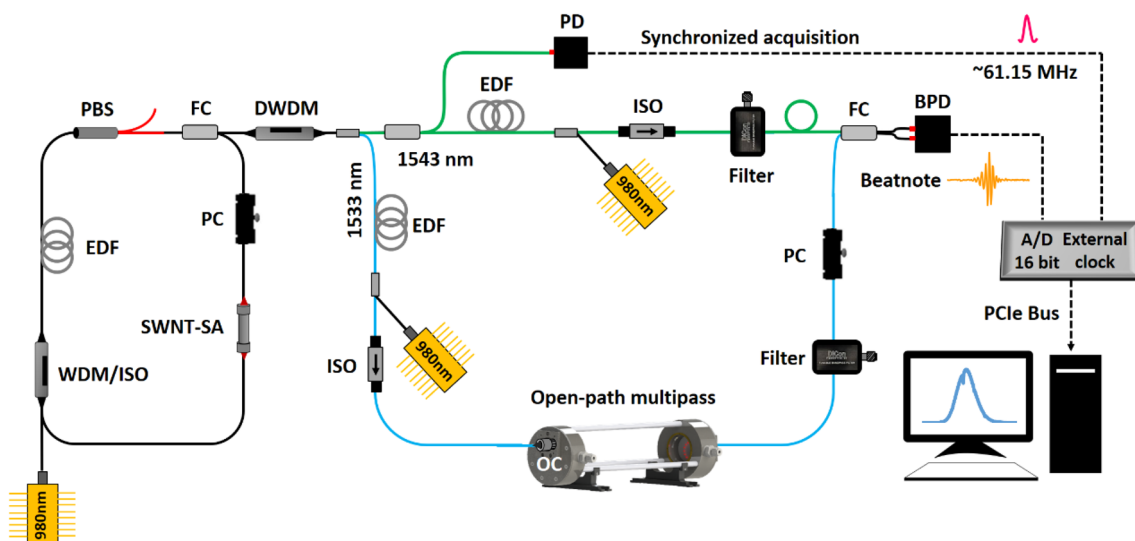


Fig. 1 Schematic of the multipass dual-comb gas sensor using a single free-running fiber laser. WDM wavelength division multiplexing, ISO isolator, EDF erbium-doped fiber, PC polarization controller, SWNT-SA single-wall nanotube saturable absorber, PBS polarization

beam splitter, FC fiber coupler, DWDM dense wavelength division multiplexing, OC optical coupler, PD photodetector, BPD balanced photodetector

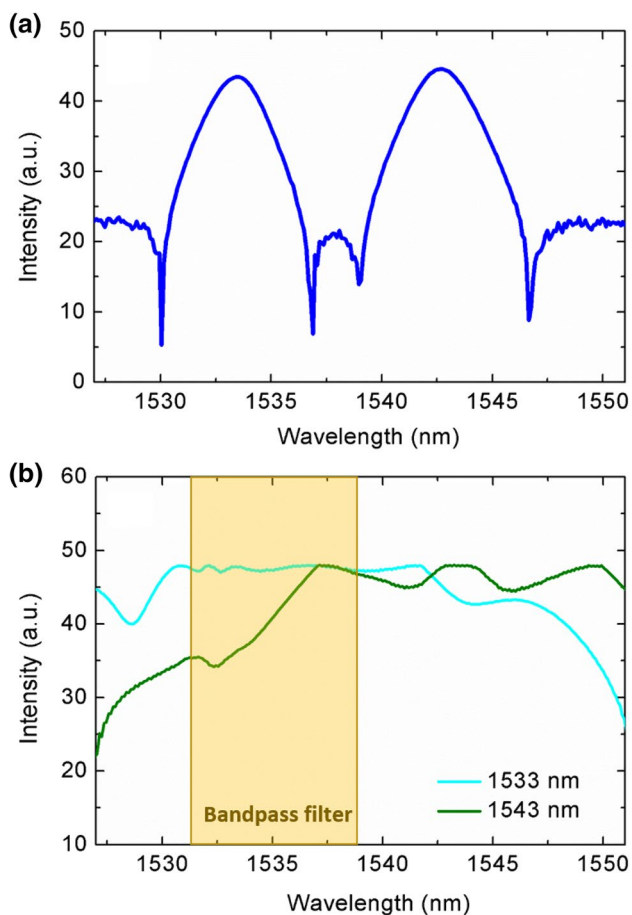


Fig. 2 **a** Emission spectrum of the dual-wavelength fiber laser. **b** Amplified and broadened comb pulse trains centered at 1533 nm and 1543 nm; the spectral window determined by the bandpass filter is indicated by the shaded region

amount. Note that the frequency difference could be varied by changing either the intracavity dispersion or the center-wavelength separation [26]; and the current dual-wavelength fiber-laser achieves a minimum Δf of 190 Hz.

The generated two comb pulse trains were then divided by a two-stage dense wavelength division multiplexer (DWDM) to form the two arms of an interferometer. The laser pulse in each arm was amplified by an EDF amplifier pumped by a 980 nm continuous-wave laser. Thus each pulse train was broadened to the spectral bandwidth of the EDF due to the strong nonlinear effect [22]. In this work the 1533-nm and 1543-nm pulses were amplified to 20.8 mW and 18.1 mW, respectively. Figure 2b depicts the spectral overlap between these two comb trains achieved in this study. Additionally, two tunable bandpass spectral filters (Dicon TF1550-3.2) with a 3.2 nm bandwidth were used in both optical arms to prevent the possible aliasing issues [27].

To improve the sensitivity of this sensor system, the 1533-nm pulse beam was delivered by a fiber collimator

into an open-path multipass cell composed of two concave mirrors (radius of curvature, 20 cm) separated by 13.5 cm. Gas samples were introduced into this open-path multipass cell without the need of any additional sampling devices [28]. After traveling 4 m inside the multipass cell, the transmitted laser pulse was coupled into the optical fiber with a controlled polarization state for coherent detection. We obtained a laser power of ~ 1 mW in the 1533-nm arm after 29 times reflections in the multipass cell as the mirror has a reflectivity of 96.6% near the laser wavelength. Hence, the laser powers in both arms were attenuated to ~ 20 μ W to keep power balance and prevent nonlinear effects in photo-detection. Both pulse trains were finally combined by a 3-dB fiber coupler for interferogram generation and detected by an InGaAs balanced photodetector (Thorlabs PDB425C).

Instead of the continuous data acquisition with a preset sampling rate [22], the synchronized acquisition technique was used to acquire more interferograms with the limited on-board memory. As illustrated in Fig. 1, a portion of the reference pulse train (1543 nm) generated from a 20:80 fiber coupler was used as an external clock to trigger the data acquisition card (Fctec Technology PCIe9801). Although the repetition frequencies of both pulse trains generated from the free-running fiber laser may drift with time, it is known that the difference Δf of the repetition frequencies remains constant [22]. Thus the interferograms could be sampled at the repetition frequency of the pulse train at 61.15 MHz and a complete interferogram could be acquired at an acquisition time of 1 ms ($1/\Delta f$). With this synchronized acquisition method, the real-time f_r triggers the acquisition of every beatnote signal that is needed to compose the interferogram no matter the possible drift of the repetition frequency. Compared with the continuous data acquisition method using a fixed sampling rate based on Shannon–Nyquist theorem, the current synchronized acquisition method effectively reduces redundant information and saves data acquisition time. Finally, the acquired interferograms were Fourier-transformed to retrieve the spectral information.

3 Results and discussion

To test the dual-comb sensor performance, the multipass gas cell was placed in a testing chamber filled with well-controlled gas mixtures. The gas chamber was designed to create a stabilized testing environment where the gas concentration and pressure were known. The multipass cell was linked with the dual-comb sensor by two 3-m long single-mode fibers to enable remote detection.

We first investigated the influence of spectral averaging on the signal-to-noise ratio (SNR) by measuring 0.1% C_2H_2/N_2 at 1 bar. Figure 3 compares the representative absorption spectra with different averaging times of the

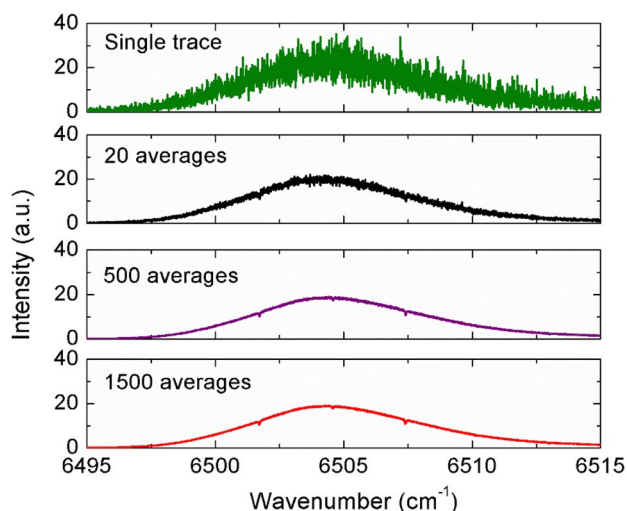


Fig. 3 Fourier-transformed spectra of 0.1% C_2H_2/N_2 obtained with different averaging times

Fourier-transformed spectra near the central wavelength 1537 nm. All the spectral data were obtained by averaging the absolute values in the Fourier-transformed spectral domain. Additional phase unwrapping was used to apply a complex multiplication of each Fourier-transformed interferogram with the unwrapped phase values. Although hardly identified from a single-shot trace, the absorption features of 0.1% C_2H_2 from 6495 to 6515 cm^{-1} become more evident with the averaging time increased from 20 to 1500.

Figure 4 plots the relationship between the spectral SNR and the averaging time. Here the spectral SNR is defined as the inverse of noise standard deviation of the spectral curve

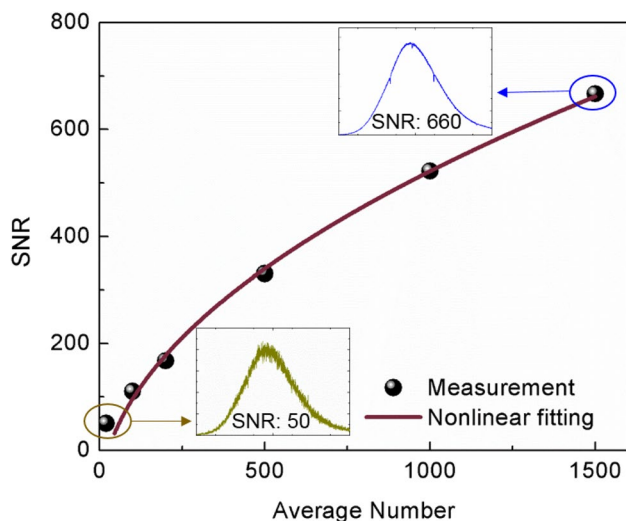


Fig. 4 Dependence of the SNR on the number of spectral averaging. The curve-fitting indicates the spectral SNR increases with the square root of the average number

(here the relatively uniform spectral range 6505–6506 cm^{-1}) normalized by the corresponding average magnitude. It is evident that the spectral SNR increases almost linearly with the square root of averaging time. The SNR improves by a factor of > 10 when the averaging time increases from 20 to 1500. Note that the acquisition of 1500 interferograms corresponds to the sample time of 1.5 s when using the synchronized acquisition technique.

To obtain the absorbance for inferring gas concentration, the absorption-free baseline is required based on Beer's law. However, such a baseline is normally unavailable in practical open-path gas sensing applications. Due to the wide spectral coverage of DCS, it is possible to extrapolate the baseline based on the obtained non-absorbing spectral region. Here we retrieved the spectral baseline by fitting the measured spectrum with the shape approximation of the optical band-pass filter [23].

Different from the DCS using a pair of OFCs with the phase locked to an external cavity or clock, our dual-comb sensor was not locked to the known standard laser frequency as a reference. Thus it is impossible to determine the absolute frequency of each comb line. To convert the RF absorption features to the corresponding absorption lines in optical domain, a priori knowledge of the spectral range determined by the bandpass filter and the positions of line-centers from HITRAN database [29] was used to calibrate the optical frequency.

Figure 5 presents the measured absorption spectra of C_2H_2 at different pressures in the frequency range 6503–6530 cm^{-1} after 1500 averages. Figure 5a–c compare the measured absorbance of 0.1% C_2H_2 with the inverted spectral simulation based on HITRAN database at 0.1, 0.2 and 1 bar, respectively. Relatively good agreement is found

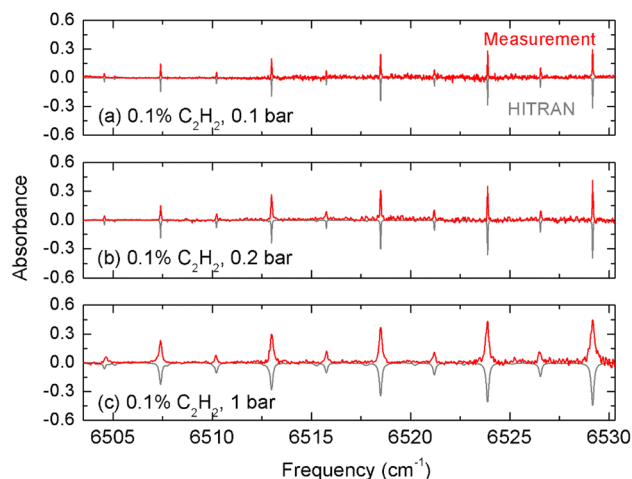


Fig. 5 Comparison of the measurement of C_2H_2 using the dual-comb sensor with the spectral simulation using HITRAN database at different pressures (0.1 bar, 0.2 bar and 1 bar)

between the measured and simulated peak values under all conditions. The standard deviations of the peak values between the measurements and the HITRAN simulations at 0.1 bar, 0.2 bar and 1 bar are determined to be 1.3%, 1.6%, and 1.2%, respectively. The pressure-broadening effect of the absorption line was well captured by the dual-comb sensor. For instance, the full width at half maximum (FWHM) of the C_2H_2 line at 6518.48 cm^{-1} is measured to be 0.037 cm^{-1} at 0.1 bar shown in Fig. 5a, which is broadened to 0.079 cm^{-1} at 0.2 bar (Fig. 5b) and 0.162 cm^{-1} at 1 bar (Fig. 5c). Similarly, the absorption features of 1% NH_3/N_2 were measured at different pressures using the same dual-comb sensor with the results of 1500 averages illustrated in Fig. 6. Again, good agreement of the peak values is seen between the measurements and HITRAN simulations.

Finally, we performed the simultaneous measurement of C_2H_2 and NH_3 with varied mixing ratios. Compared with the atmospheric pressure, the sensor system operating at lower pressures may take advantages of distinguishable absorption lines for gas analysis. Thus all the experiments were conducted at 0.1 bar with 1500 spectral averages. With the C_2H_2 concentration varied from 400 to 700 ppm and NH_3 varied from 0.5 to 0.2% at the same time, Fig. 7 depicts two of the measured absorbance profiles. By comparing with the inverted HITRAN simulation of C_2H_2 and NH_3 illustrated in Fig. 7, the absorption lines of C_2H_2 and NH_3 are clearly distinguished in the spectral range from 6503 to 6530 cm^{-1} .

We are able to infer the gas compositions by performing the least-squares spectral fitting to the measured peak values. Based on the peak positions provided by the HITRAN database, we only set the concentrations of C_2H_2 and NH_3 as variables in the fitting process, while keeping all the other parameters such as temperature, pressure and absorption

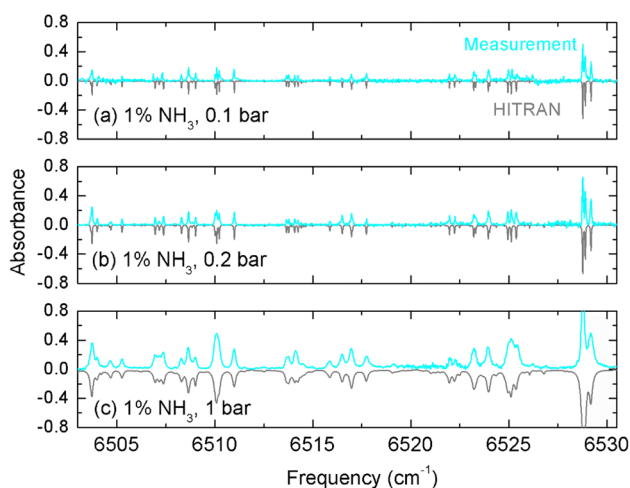


Fig. 6 Comparison of the measurement of NH_3 using the dual-comb sensor with the spectral simulation using HITRAN database at different pressures (0.1 bar, 0.2 bar and 1 bar)

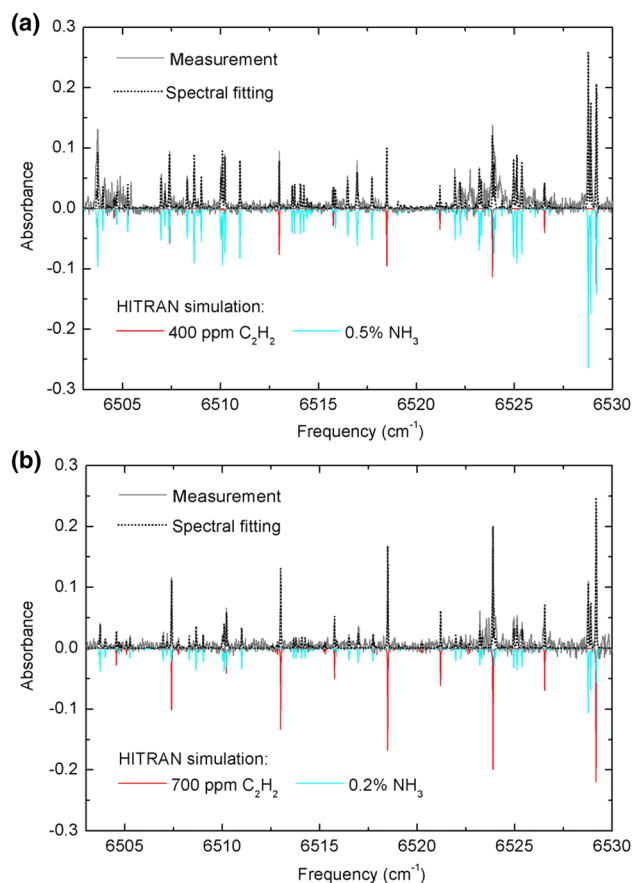


Fig. 7 Comparison of the measured and simulated absorption profiles of $C_2H_2/NH_3/N_2$ mixtures at 0.1 bar with different mixing ratios. **a** 400 ppm C_2H_2 and 0.5% NH_3 ; **b** 700 ppm C_2H_2 and 0.2% NH_3

length as the fixed values. For instance, the C_2H_2 and NH_3 concentrations in Fig. 7a were determined to 411 ppm and 0.495%, respectively; and the gas mixture shown in Fig. 7b were determined to be 693 ppm C_2H_2 and 0.205% NH_3 , respectively. The deviation of the DCS-determined concentrations from the nominal values is within 3%. We also observed a background noise corresponding to an absorbance level of 0.01 that serves as the detection limit of the current dual-comb sensor. Hence, further research is needed to investigate the methods of reducing the background noise both in the hardware and software.

4 Conclusions

We reported a multipass-assisted dual-comb gas sensor for the simultaneous and sensitive C_2H_2 and NH_3 detection using a single free-running erbium-doped fiber laser. With the two comb pulse trains emitted from the same cavity, the dual-comb system ensures mutual coherence without using complex and expensive electronic feedback

systems. A multipass design was used to increase the detection sensitivity. The DCS-determined absorption features of C_2H_2 and NH_3 at 0.1–1 bar were in excellent agreement with the HITRAN simulation over the spectral range 6503–6530 cm^{-1} . The free-running fiber laser without the need of any locking schemes makes our proposed DCS gas sensor promising for field applications. Although demonstrated for C_2H_2 and NH_3 sensing in the present work, the current DCS sensor could be extended to other molecules using different doped fiber materials or nonlinear optical fiber broadening for a broader spectral coverage [30]. Future work is suggested to investigate the methods of reducing the background noise in the comb source to further enhance the detection sensitivity.

Acknowledgements This research is supported by National Natural Science Foundation of China (51776179, 61435002, 61675014, 61675015).

References

1. T. Udem, R. Holzwarth, T.W. Hänsch, *Nature* **416**, 233 (2002)
2. S.T. Cundiff, J. Ye, *Rev. Mod. Phys.* **75**, 325 (2003)
3. T.W. Hänsch, *Rev. Mod. Phys.* **78**, 1297 (2006)
4. N. Picqué, T.W. Hänsch, *Nat. Photon.* **13**, 146 (2019)
5. S.A. Diddams, L. Hollberg, V. Mbele, *Nature* **445**, 627 (2007)
6. C. Gohle, B. Stein, A. Schliesser, T. Udem, T.W. Hänsch, *Phys. Rev. Lett.* **99**, 263902 (2007)
7. S. Schiller, *Opt. Lett.* **27**, 766 (2002)
8. I. Coddington, N. Newbury, W. Swann, *Optica* **3**, 414 (2016)
9. T. Ideguchi, A. Poisson, G. Guelachvili, N. Picqué, T.W. Hänsch, *Nat. Commun.* **5**, 3375 (2014)
10. I. Coddington, W.C. Swann, N.R. Newbury, *Phys. Rev. Lett.* **100**, 013902 (2008)
11. P. Giaccari, J.-D. Deschênes, P. Saucier, J. Genest, P. Tremblay, *Opt. Express* **16**, 4347 (2008)
12. J. Roy, J.-D. Deschênes, S. Potvin, J. Genest, *Opt. Express* **20**, 21932 (2012)
13. T. Yasui, R. Ichikawa, Y.-D. Hsieh, K. Hayashi, H. Cahyadi, F. Hindle, Y. Sakaguchi, T. Iwata, Y. Mizutani, H. Yamamoto, K. Minoshima, H. Inaba, *Sci. Rep.* **5**, 10786 (2015)
14. S. Potvin, S. Boudreau, J.-D. Deschênes, J. Genest, *Appl. Opt.* **52**, 248 (2013)
15. X. Zhao, Z. Zheng, L. Liu, Y. Liu, Y. Jiang, X. Yang, J. Zhu, *Opt. Express* **19**, 1168 (2011)
16. T. Ideguchi, T. Nakanura, Y. Kobayashi, K. Goda, *Optica* **3**, 748 (2016)
17. S. Mehravar, R.A. Norwood, N. Peyghambarian, K. Kieu, *Appl. Phys. Lett.* **108**, 231104 (2016)
18. S.M. Link, D.J.H.C. Maas, D. Waldburger, U. Keller, *Science* **356**, 1164 (2017)
19. X. Zhao, T. Li, Y. Liu, Q. Li, Z. Zheng, *Photon. Res.* **6**, 853 (2018)
20. Y. Nakajima, Y. Hata, K. Minoshima, *Opt. Express* **27**, 5931 (2019)
21. M.I. Kayes, N. Abdurkerim, A. Rekikand, M. Rochette, *Opt. Lett.* **43**, 5809 (2018)
22. X. Zhao, G. Hu, B. Zhao, C. Li, Y. Pan, Y. Liu, T. Yasui, Z. Zheng, *Opt. Express* **24**, 21833 (2016)
23. R. Liao, Y. Song, W. Liu, H. Shi, L. Chai, M. Hu, *Opt. Express* **26**, 11046 (2018)
24. Y. Zhao, C. Shu, *Appl. Phys. Lett.* **72**, 1556 (1998)
25. P.C. Becker, N.A. Olsson, J.R. Simpson, *Erbium-doped fiber amplifiers: fundamentals and technology* (Academic Press, San Diego, 1999)
26. H. Zhang, D.Y. Tang, X. Wu, L.M. Zhao, *Opt. Express* **17**, 12692 (2009)
27. I. Coddington, W.C. Swann, N.R. Newbury, *Phys. Rev. A* **82**, 043817 (2010)
28. A. Foltynowicz, P. Maslowski, T. Ban, F. Adler, K.C. Cossel, T.C. Briles, J. Ye, *Faraday Discuss.* **150**, 23 (2011)
29. I.E. Gordon, L.S. Rothman, C. Hill, R.V. Kochanov, Y. Tan, P.F. Bernath, M. Birk, V. Boudon, A. Campargue, K.V. Chance, B.J. Drouin, J.M. Flaud, R.R. Gamache, J.T. Hodges, D. Jacquemart, V.I. Perevalov, A. Perrin, K.P. Shine, M.A.H. Smith, J. Tennyson, G.C. Toon, H. Tran, V.G. Tyuterev, A. Barbe, A.G. Császár, V.M. Devi, T. Furtenbacher, J.J. Harrison, J.M. Hartmann, A. Jolly, T.J. Johnson, T. Karman, I. Kleiner, A.A. Kyuberis, J. Loos, O.M. Lyulin, S.T. Massie, S.N. Mikhailenko, N. Moazzen-Ahmadi, H.S.P. Müller, O.V. Naumenko, A.V. Nikitin, O.L. Polyansky, M. Rey, M. Rotger, S.W. Sharpe, K. Sung, E. Starikova, S.A. Tashkun, J.V. Auwera, G. Wagner, J. Wilzewski, P. Wcisło, S. Yu, E.J. Zak, *J. Quant. Spectrosc. Radiat. Transf.* **203**, 3 (2017)
30. J. Chen, X. Zhao, Z. Yao, T. Li, Q. Li, S. Xie, J. Liu, Z. Zheng, *Opt. Express* **27**, 11406 (2019)

Publisher's Note Springer Nature remains neutral with regard to jurisdictional claims in published maps and institutional affiliations.